Supplementary Information

A Giant Hybrid Organic-Inorganic Octahedron from a Narrow Rim Carboxylate Calixarene

Fernando Machado dos Santos,[a] Meiry Edivirges Alvarenga,[a] Ana Karoline Silva Mendanha Valdo,[a] Renato Rabelo,[b] Danielle Cangussu de Castro Gomes,[a] Ângelo de Fátima,[c] Thiago Vinicius Costa Lara,[c] Cleiton Moreira da Silva,[c] Thiago Teixeira Tasso,[c] João Honorato Araujo Neto,[d] Alzir Azevedo Batista,[d] Alejandro Pedro Ayala,[e] Javier Alcides Ellena,[f] Vinicius Ferraz Guimarães,[a] Cecília Maria Alves Oliveira,[a] Lidya Cardozo da Silva,[a] Boniek Gontijo Vaz,[a] and Felipe Terra Martins*[a]

[a] Institute of Chemistry, Federal University of Goias, CP 131, 74001-970, Goiania, GO, Brazil.

[b] Institute of Molecular Science (ICMol), University of Valencia, 46980 Paterna (Valencia), Spain.

[c] Department of Chemistry, Federal University of Minas Gerais, 31270-901, Belo Horizonte, MG, Brazil.

[d] Department of Chemistry, Federal University of Sao Carlos, 13565-905, Sao Carlos, SP, Brazil.

[e] Department of Physics, Federal University of Ceara, CP 6030, 60455-970, Fortaleza, CE, Brazil.

[f] São Carlos Institute of Physics, University of São Paulo, CP 369, 13560-970, Sao Carlos, SP, Brazil.

E-mail: felipe@ufg.br

Content:

1. Synthesis…….....…2
2. Single Crystal X-Ray Diffraction…….……..3
3. Mass spectrometry and elemental analysis...…….5
4. WDS…….…….…7
5. Magnetic properties and X-band EPR spectra ……..…7
6. Description of **3** and **4** and Magnetic Properties of **4**……....8
7. Table…….……13
8. Figures ……...…….14
9. References……..……...…….……..25
10. Author Contributions……...26
11. Acknowledgments……....26

1. Synthesis

The reagents were of analytical grade, purchased from Sigma-Aldrich Corp. and used without further purification. The synthesis of NaH_3**L** was performed as described earlier by us,[1] as follows. Commercially acquired calix[4]arene (1.00 g, 11.8 mmol), ethyl bromoacetate (7.88 g, 47.2 mmol) and Na_2CO_3 (5.00 g, 47.2 mmol) were refluxed in 50 mL of dry acetone for 24 h. After removing the solvent, the crude mixture was dissolved in a mixture comprising ethanol (20 mL) and water (20 mL), and NaOH (4.00 g, 100 mmol) was added. The reaction mixture was heated to reflux for 24 h. Then, the cooled solution was acidified with 2.0 mol L^{-1} HCl up to pH 1, followed by immediate precipitation of a white solid which was filtered and washed with water several times. Next, this solid was dissolved in ethyl acetate and the organic solution was washed with 20% HCl aqueous solution (twice) and water (three times) to withdraw impurities. The organic phase was then dried over $MgSO_4$ and concentrated, yielding NaH_3**L** as a residual white solid. Its ESI(+) mass spectrum is shown in Figure S7 and its elemental analysis was [% Found (% Calc.) for $C_{36}H_{31}NaO_{12}$ (MW = 678.61)]: C, 63.53 (63.72); H, 4.64 (4.60).

The barium, copper and zinc complexes were synthesized following the methodology described previously.[1] Reagents ratio was changed in the crystallization screening, and those stoichiometric amounts outputting crystals of **1-4** are described in sequence.

For the synthesis of **1**, 0.040 mmol (27.1 mg) of sodium tetra(carboxymethoxy)calix[4]arene was dissolved in DMSO (3 mL), which was mixed with 10 μL of 1.0 mol L^{-1} $ZnSO_4$ (0.010 mmol, 1.6 mg). For **2**, the calixarene amount was 6.8 mg (0.010 mmol), also dissolved in 3 mL of DMSO, followed by addition of 27

μL of 1.0 mol L^{-1} $Zn(CH_3CO_2)_2 \cdot 2H_2O$ (0.027 mmol, 5.9 mg) aqueous solution, respectively. A NaCl amount of 0.6 mg (0.010 mmol) was dissolved in the mixture already containing the calixarene and the zinc salt. The synthesis of **3** and **4** involved dissolution of sodium tetra(carboxymethoxy)calix[4]arene (0.020 mmol, 13.6 mg) in DMSO (3 mL). This solution was carefully mixed with 10 μL of 1.0 mol L^{-1} $BaCl_2$ (0.010 mmol, 2.1 mg) and 10 μL of 1.0 mol L^{-1} $CuCl_2$ (0.010 mmol, 1.3 mg) aqueous solutions, respectively. After one month of slow evaporation, at room temperature, single crystals of **1**, **3** and **4** were isolated from mother solution, while crystals of **2** were formed after ca. 6 months upon standing.

2. Single Crystal X-Ray Diffraction

Single-crystal X-ray diffraction data were measured using either a Bruker-AXS D8 Venture κ-geometry diffractometer (**1** and **2**), equipped with a Photon II CMOS detector and a IμS 3.0 Incoatec microfocus source (Cu Kα) and an Oxford Cryostream cryostat (800 series Cryostream Plus, 90(2) K), or a Bruker-AXS Kappa Duo diffractometer (**3** and **4**), equipped with an APEX II CCD detector and Mo Kα or Cu Kα microfocus sources, at room temperature (296(2) K). Cell indexing and intensity dataset processing were performed with Bruker programs SAINT and SADABS.[2] All datasets were corrected for absorption (Multi-scan).[3] Structure solution and refinements were done using SHELXS and SHELXL,[4] respectively, within the WinGX[5] and OLEX2[6] software packages. ORTEP-3[5] and Diamond[7] were used to structure view, interpretation and drawing. Non-hydrogen and hydrogen atoms were treated in the refinements as anisotropic and isotropic, respectively.

Smeared electronic density peaks were also found in the difference Fourier map of **1** and **2**, which can be probably non-stoichiometric solvent molecules. However,

their assignment was not possible and their contribution to the scattering was removed in both datasets using the solvent mask tool available in OLEX2[6], and then not reporting them in the molecular weight shown in Table S1. In fact, both the best dataset for **1** and **2** were acquired at 90 K. Furthermore, low-quality crystals and symmetry impositions of the *Ibam* space group in **2** have precluded the data quality, outputting so not satisfactory refinement statistics even acquiring X-ray diffraction data at temperature of 90 K on a CMOS detector. In addition, complementary high-resolution mass spectrometry technique aided us to support such assignment. To the best of our knowledge, these low-ordering phenomena and the derived unsatisfactory refinement statistics are very common in crystal structure determination of calixarenes.[8]

DFIX restraint was employed to seventeen bond lengths into the carboxymethoxy legs of **1**, and in one Na-O distance, as well as FLAT restraint was also used to keep planar the atoms of two carboxylate groups in this structure. In **2**, DFIX restraints were employed to six bond lengths of two phenyl rings, five bond lengths of a carboxymethoxy leg and two bonds of a DMSO, where one DANG restraint was also applied. Atomic displacement parameters (ADPs) of five carboxylate oxygens, two water oxygens, and three carboxymethoxy carbons were also constrained in **2**, using the EADP command, which was also applied to six carbon and fourteen oxygen sites belonging to carboxymethoxy legs of **1**. EADP and EXYZ commands were also used to the two mixed sites sharing Na^{+} and Zn^{2+} at equal 50% occupancy in **2**.

In **1** and **2**, carboxylic/carboxylate groups were disordered over two sites of occupancy, respectively. Seven groups in **1** and four carboxylate moieties in **2** were disordered and their occupancy values were found in trial refinements and then constrained or refined freely. In addition, in **2** two disordered groups had atoms close to special positions and then should have equal occupancies. The EADP constraint was

also applied to methylene and carboxylic carbons in **4** and to methyl carbons of four DMSO molecules in **3**. In the former, DFIX and DANG restraints were employed to bond lengths belonging to three DMSO molecules.

Inversion twin law was found for **4** with ROTAX,[9] and the refined minor domain contribution was 12%. SIMU (**1**-**4**), RIGU (**1**, **2**) and DELU (**4**) restrained also ADPs of non-hydrogen atoms in the refinements. All CH hydrogens were placed according to expected valence angles and lengths, and their coordinates were constrained during refinements, oscillating as changes in the freely refined bonded carbon coordinates. All OH and water hydrogens were seen in the difference Fourier map and then fixed during refinements. In carboxylic groups, C—O bond lengths were helpful to assign the proton position, always keeping satisfactory intramolecular and intermolecular hydrogen bond geometry and network. The isotropic hydrogen displacement parameters were set to $1.2U_{iso}$(C/N) or $1.5U_{iso}$(O/C_{methyl}). The entire X-ray diffraction dataset is available for **1-4** under CCDC deposit codes 2000511, 2000512, 1859264 and 1876681, respectively.

3. Mass spectrometry and elemental analysis

The crystalline products were dissolved in methanol to a concentration of 10 μg mL^{1}. ESI - MS analyses were performed on a microQTOF-Q III (Bruker Daltoniks, GmbH) in full scan mode by direct infusion at a flow rate of 4 mL min^{-1}. The electrospray source was operated using high purity nitrogen as desolvation, nebulizer, and collision gas. For desolvation, the temperature was kept at 200 °C and the flow at 3.8 L min^{-1}, and the nebulizer pressure was kept at 0.3 bar.

The analyses were performed in positive mode with capillary voltage set at the range of 3500-4500 V. The Q-TOF conditions were as follows: End Plate Offset: -500

V; Funnel 1: 300-400 Vpp; Funnel 2: 400-450 Vpp; Hexapole RF: 400-450 Vpp; Collision RF: 650 Vpp; Transfer Time: 50-100µs; Pre Pulse Storage: 12-20 µs; Ion Energy Quadrupole: 5 - 25 eV; Rolling Average: 2 x 1Hz. The mass spectra were acquired and processed, respectively using, otofControl and Bruker Compass DataAnalysis Softwares (Bruker Daltonik, GmbH).

MALDI-TOF MS spectra were obtained in a Bruker Autoflex III smart bean spectrometer, equipped with a modified Nd:YAG laser (330-360, 495-540, 808, 990-1080 nm). The measurements were performed in the positive mode using linear configuration, with the following parameters: ion source voltage 1 of 16.6 kV, ion source voltage 2 of 9 kV, 300 laser shots per spectrum at a 100 Hz rate. DCTB (trans-2-[3-(4-*tert*-butylphenyl)-2-methyl-2-propenylidene]malononitrile), dissolved in dichloromethane (0.1 mg/mL), was used as matrix and applied at the spot containing the calixarene samples in DMSO on the stainless steel plate.

MALDI-TOF spectra can be obtained in the linear or reflectron configurations. In the latter, good resolution is obtained because ionized species are focused by means of a reflector TOF setup. However, some large molecules as proteins, for example, are not stable enough to endure the energetic stress which is inherited of passing the reflector. This was apparently the case of giant calixarene **2**, which yielded no signal in the 2,000 – 10,000 *m/z* range in the reflectron configuration.

The linear setup usually solves stability problems; however, resolution is lost because ions of identical mass arrive at the detector at slightly different times causing peak broadening. Hence, no isotope distribution could be observed in the mass spectrum of **2**, as easily seen in the inset of Figure 3. Still, sharp and intense signals in the *m/z*

5700 region appeared, corroborating with the $(C_{36}H_{28}O_{12})_6(H_2O)_{13}Na_{12}Zn_{16}O_8(OH)_4$ molecular formula proposed by the crystallography and WDS analyses.

Optimum visualization of the molecular ion species in the spectrum was achieved in concentrated solutions of **2** in DMSO and when the laser intensity was set to a minimum threshold necessary for ionization (35% in our case), preserving the integrity of the structure. Deposition of DCTB on the spot followed by the sample led to a spectrum with better signal to noise ratio compared to the opposite application order. The use of acid matrixes, such as super DHB and α-cyano-4-hydroxycinnamic acid, resulted only in broad signals with very poor resolution (data not shown), probably due to disruption of the giant calixarene structure by protonation of carboxylate and hydroxyl moieties.

Elemental analysis of NaH_3**L** was carried out using an EA-1108 CHNS FISONS element analyzer at the Microanalytical Service of the Federal University of Sao Carlos.

4. Wavelength-dispersive X-ray spectroscopy (WDS) spectroscopy

Wavelength-dispersive X-ray spectroscopy (WDS) was performed on a JEOL JXA-8230 electron microprobe equipped with five WDS detectors and crystals LDE1, LDE2, TAP, PET/L-H and LIF-L/H. The analytical setup was: 15 kV and 20 nA, 2 μm spot size and the signal accumulation time was 10 seconds for zinc and sodium.

5. Magnetic properties and X-band EPR spectra

X-band EPR spectra of a polycrystalline sample of **4** were recorded as a function of the temperature under non-saturating conditions with a Bruker ER 200 D spectrometer equipped with a helium-flow cryostat. Variable-temperature (2.0–250 K) direct current (dc) magnetic susceptibility measurements under applied fields of 0.25 (T< 20 K) and 5.0 kG (T> 20 K) were carried out on a polycrystalline simple of **4** with a

Quantum Design SQUID magnetometer. The magnetic susceptibility data were corrected for the diamagnetism of the constituent atoms and the sample holder.

6. Description of 3 and 4 and Magnetic Properties of 4

Calix[4]tubes have been discovered recently as discrete or polymeric tube-shaped entities formed by tail-to-tail dimerization of partially deprotonated $H_4\mathbf{L}$ together with simultaneous narrow rim binding to three sodium ions.[1] Next, calix[4]tube was used as platform of small molecule cocrystallization, revealing its applicability into molecular host-guest chemistry besides entrapping alkali ions.[10] Concerning sodium binding in the known discrete Na_3 calix[4]tubes, one alkali ion is present into the narrow rim cavity of each $H_3\mathbf{L}^-$ or $H_2\mathbf{L}^{2-}$ unit, being surrounded by the four phenoxy oxygens and other four carboxylic/carboxylate oxygens. The third sodium is shared between the two units, being bound to carboxylic/carboxylate oxygens from both units. This shared Na binding pattern is responsible for linking the two $H_3\mathbf{L}^-$/ $H_2\mathbf{L}^{2-}$ units as a tubular dimer, which is further stabilized through OH…O hydrogen bonds between carboxylate and carboxylic groups. Furthermore, polymeric chains can be formed if a fourth Na ion is bonded simultaneously to two neighboring calix[4]tubes, totalling four carboxylate groups per dimeric assembly.

When barium chloride (0.010 mmol) was reacted with $NaH_3\mathbf{L}$ (0.010 mmol), the discrete Na_2Ba calix[4]tube (**3**) was obtained. It presented two sodium ions and one barium, as already described in the crystal structure of a literature analog.[11] However, while in this literature compound barium is bonded to phenoxy oxygens of both calixarene units, and sodium ions are lodged into the major hydrophobic cavity, in our structure, the barium ion replaced the central sodium ion found in a Na_3 calix[4]tube, changing also the protonation pattern of carboxylic groups to balance the overall

charge. Interestingly, two crystallographically independent calix[4]tubes, labeled as A and B in Figure S8, were present, possessing different Ba^{2+} binding patterns and tube conformations. While Ba^{2+} is bonded only to oxygens from acid tails in tube B, two water oxygens and one oxygen from DMSO are interacting with Ba^{2+} in tube A (Figures S8 and S9). The result is a straight tube structure for B, while A is bent-shaped due to the inclined orientation of the $H_2\mathbf{L}^{2-}$ units.

It is worth noting that all calixarene units of **3** have one enclosed sodium counterion in its minor cavity formed at the narrow rim, as already reported for our inspiring Na_3 calix[4]tube.[1] Nevertheless, among all calix[4]tubes already known and those reported here, **3** is the first example present with four carboxylate groups in a same calixarene unit, as well as it is the first case with four carboxylic groups in a same $H_4\mathbf{L}$ unit. There are four carboxylate groups in the Na_2Ba calix[4]tubes, and interestingly, in the molecule labelled as B, these belong to a same calixarene unit. In all other known calix[4]tubes and in the others to be described here, partial deprotonation of subunits occurs. It is important to state that the assignment of acid hydrogens was based mainly on the C-O bond lengths into carboxylic groups, even though residual electron density peak in the difference Fourier map and intermolecular hydrogen bonding geometry were also criteria for localizing such hydrogens. In this Na_2Ba calix[4]tube, labelled as molecule B, there are four carboxylic acid hydrogen bonds sealing the tube at its central region. All its three ions are bonded to eight oxygens in square antiprismatic geometry, being that the $H_4\mathbf{L}$ and $\mathbf{L}^{4-}$ units are tail-to-tail arranged coherently.

In the Na_2Ba calix[4]tube labelled as molecule A, six oxygens from acid tails, three of each $H_2\mathbf{L}^{2-}$ subunit, complete the nine-coordinated tricapped trigonal prismatic environment of Ba^{2+} together with two water oxygens and one DMSO. Concerning

hydrogen bonds sealing the tube A at its central region, there are two contacts between carboxylic and carboxylate groups at the concave side of the bent-shaped tube. At the convex side of tube A, where water and DMSO molecules are bonded, hydrogen bonds contributes for structure stabilization. This can be viewed mainly in the intramolecular hydrogen bonding donation from one water molecule to two carboxylate oxygens from distinct $H_2\mathbf{L}^{2-}$ units. Another water molecule is both intramolecular and intermolecular hydrogen bonding donor to two carboxylate oxygens (Figures S8 and S9). Each $H_2\mathbf{L}^{2-}$ unit has also one carboxylic group pointed outwards the tube A backbone, being interacted with either lattice water or DMSO molecule. Besides the two water and one DMSO molecules bonded to Ba1, there are also six water and four DMSO molecules in the crystal lattice of Na_2Ba calix[4]tube. Furthermore, such a conformational change of two acid tails results in a seven-coordinated capped trigonal prismatic environment of both Na^+ ions in tube A. Interestingly, tube A has DMSO molecule entrapped into its both hydrophobic cavities through C-H…π contacts, while these two cavities of tube B are hosting phenyl groups from neighboring tubes A through π…π interactions (Figure S9), as in the parent sodium calix[4]tubes.[1]

When copper chloride (0.010 mmol) was reacted with $NaH_3\mathbf{L}$ (0.020 mmol), the Cu^{2+} ion was able to coordinate to two $H_3\mathbf{L}^-$ units, yielding compound **4**. Each $H_3\mathbf{L}^-$ unit engages its carboxylate group in the coordination to Cu^{2+}, which is also bound to two chloride ions (Figure S10). This gives rise to a square-planar geometry around Cu^{2+}. Sodium ions exhibit eight-coordinated square antiprismatic environment, being surrounded by one carboxylate, three carboxylic and four phenoxy oxygens. However, one chloride ion is aligned with sodium ions at the tube center of the Na_2Cu calix[4]tube rather than Ba^{2+} in the analogous structure. Cu^{2+} is placed more laterally within the tube,

while another chloride is at the tube periphery accepting two hydrogen bonds from acid tails belonging to a neighboring tube (Figure S11).

In **4**, four sealer intramolecular hydrogen bonds occur between carboxylic and carboxylate groups (Figure S10). Therefore, there are three carboxylic hydrogen bonding donors per $H_3\mathbf{L}^-$ unit, which indeed is present with only one carboxylate group. Another interesting observation is the isostructurality between this discrete Na_2Cu calix[4]tube and the Na_4 polymeric one.[1] In the former literature structure, there is a fourth sodium ion in lieu of chloride acting as a bridge between neighboring Na_2Cu calix[4]tubes. This keeps the same solid state packing pattern of the tubes in those structures, including the same tetragonal $P4_2bc$ space group and cell constants. Also, their asymmetric unit contains only one $H_3\mathbf{L}^-$ unit besides ions positioned on a two-fold rotation axis. In the asymmetric unit of the copper calix[4]tube reported here, there are two halves of chloride anions and one half of Cu(II) on the same 2-axis running parallel to [001], besides one entire $H_3\mathbf{L}^-$ unit and one entire DMSO molecule. The last is hosted into calixarene cavity by C-H…π interactions besides accepting two non-classical C-H…O hydrogen bonds from phenyl rings of a neighboring tube in the lattice (Figure S11), as also occurs in the precedent polymeric Na_4 calix[4]tubes present either with DMSO or DMF.[1]

Based on the highlighted magnetic properties of copper-calixarene complexes, we have also investigated the $\chi_M T$ against T plot [χ_M is the magnetic susceptibility per Cu^{2+} ion] of **4**, as shown in Figure S12. Concerning magnetic properties of **4**, at room temperature, $\chi_M T$ is equal to 0.417 cm^3 mol^{-1} K, a value which is as expected value for a magnetically isolated spin doublet ($\chi_M T$ = 0.413 with S_{Cu} = ½ and g_{Cu} = 2.10). Upon cooling, $\chi_M T$ follows a Curie law until 20 K and it further slightly decreases to 0.40cm^3 mol^{-1} K at 2.0 K. A Weiss parameter in the form of (T – θ) was introduced into the

Curie law equation for mononuclear Cu(II) complex to take into account the very weak intermolecular magnetic interactions which are responsible for the observed small decrease of $\chi_M T$ at very low temperatures. The best-fit parameters are $g_{Cu} = 2.11$ and $\theta = -0.116$ K.

The X-band EPR spectrum of a polycrystalline sample of **4** at room temperature is quasi isotropic with a signal at g = 2.12. At 4.0 K, this signal is typical of a triplet with a hyperfine splitting into seven components neatly resolved on the low field edge of the $\Delta M = 1$ transition, the seventh one appearing as a shoulder on the signal at 3270 G (inset of Figure S12). The values of the $g_{\parallel}$, $g_{\perp}$ and $A_{\parallel}$ are 2.285, 2.076 and 133 G, respectively. The sequence $g_{\parallel} > g_{\perp} > 2.0$ indicates a mainly d_{x2-y2} orbital ground state which is in agreement with the structure and the value of the peak to peak separation ($A_{\parallel}$) is in the range of those reported for hyperfine patterns in other structurally characterized copper(II) complexes.[12]

7. Table

Table S1. Crystal data and refinement statistics of **1**-**4**.

		1	**2**	**3**	**4**
Structural formula		$C_{146}H_{133}Na_5O_{52}SZn$	$C_{228}H_{250}Na_{12}O_{111}S_6Zn_{16}$	$C_{154}H_{163}Ba_2Na_4O_{59.5}S_5$	$C_{76}H_{74}Cl_2CuNa_2O_{26}S_2$
Molar weight (g/mol)		2931.90	6280.77	6985.55	1647.90
Crystal system		triclinic	orthorhombic	triclinic	tetragonal
Space group		*P*-1	*Ibam*	*P*-1	$P4_2bc$
Z		2	4	2	4
λ (Å)		1.54178	1.54178	1.54178	0.71073
T (K)		90(2)	90(2)	296(2)	296(2)
Unit cell dimensions	*a* (Å)	14.6326(2)	38.7960(16)	15.0412(4)	21.229(6)
	b (Å)	21.6788(4)	19.3541(8)	21.4819(6)	21.229(6)
	c (Å)	24.9354(4)	34.5194(12)	25.0925(6)	16.471(4)
	α(°)	79.0166(10)	90	80.748(2)	90
	β(°)	81.3602(10)	90	81.104(2)	90
	γ(°)	86.7297(10)	90	86.096(2)	90
V (Å^3)		7673.6(2)	25919.3(18)	7898.2(4)	7423(5)
Calculated Density (Mg/M^3)		1.269	1.610	1.469	1.475
Absorption coefficient (Mm^{-1})		1.198	3.064	5.354	0.517
Absorption correction		Multi-scan	Multi-scan	Multi-scan	Multi-scan
		T_{min} / T_{max} = 0.749	T_{min} / T_{max} = 0.732	T_{min} / T_{max} = 0.813	T_{min} / T_{max} = 0.865
θ-range for data collection (°)		1.823 – 73.593	2.280 – 68.520	2.086 – 66.774	2.145 – 25.060
Index ranges		-17 to 18	-45 to 46	-17 to 16	-24 to 25
		-26 to 26	-23 to 22	-25 to 20	-20 to 25
		-30 to 30	-34 to 41	-29 to 29	-18 to 19
Data collected		250,232	96,201	71,952	21,928
Unique reflections		30,390	12,107	27,026	6,596
Unique reflections with $I>2\sigma(I)$		23,077	6,441	18,185	2,378
Symmetry factor (R_{int})		0.0826	0.1795	0.0675	0.4413
Completeness to $\theta_{max.}$		98.2	99.4	96.5	99.5
F (000)		3,052	12,856	3,598	3,420
Parameters refined		1,974	941	2011	449
Goodness-of-fit on F^2		1.083	1.582	1.045	0.995
Final R_1factor for $I>2\sigma(I)$		0.1081	0.1771	0.0970	0.1164
wR2 factor for all data		0.3322	0.4770	0.3079	0.2995
Largest diff. peak / hole (*e*/Å^3)		2.320/-2.279	2.991/-2.394	2.979/-2.323	0.513/-1.557
CCDC deposit number		2000511	2000512	1859264	1876681

8. Figures

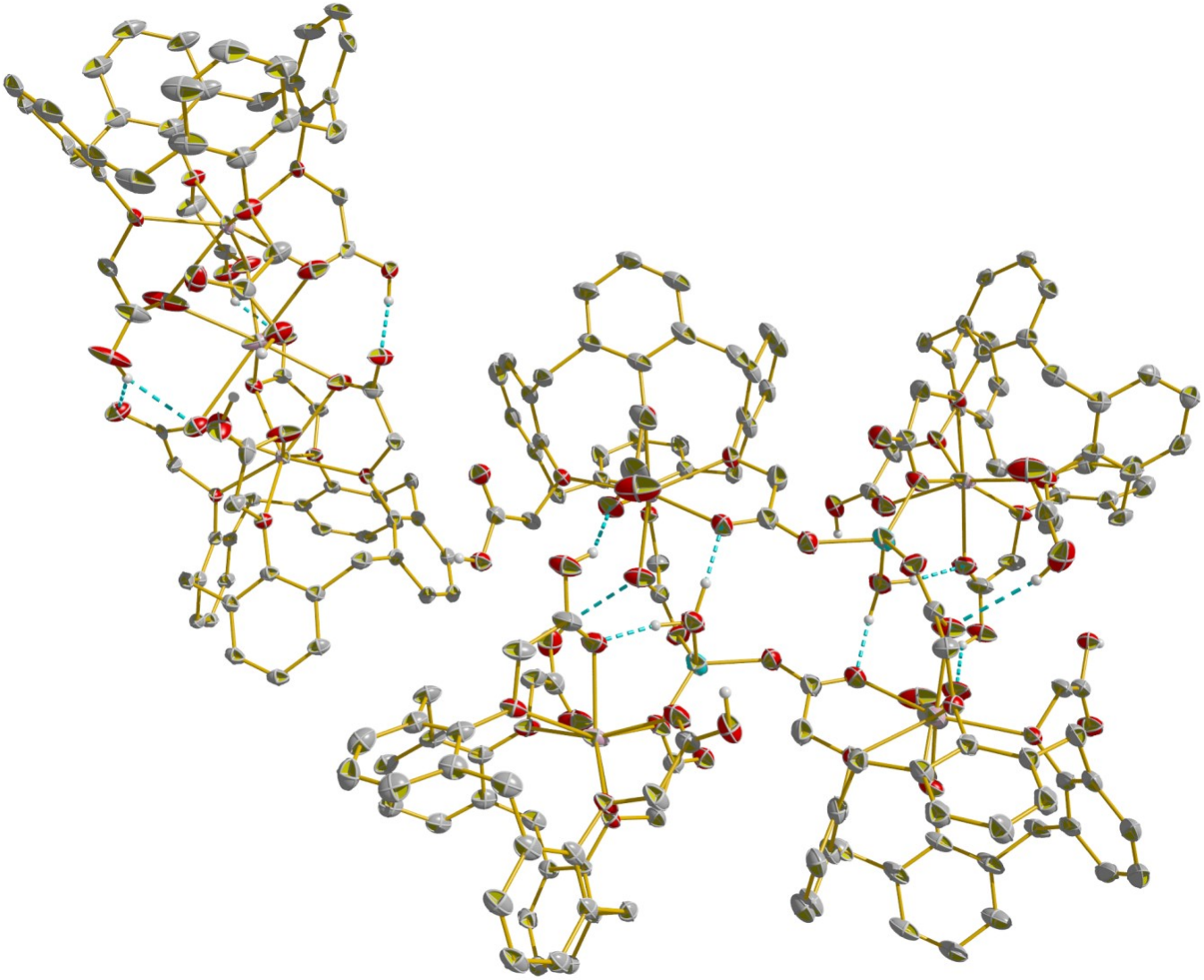

Figure S1. 50% Probability ellipsoids for non-hydrogen atoms of the tetramer **1** (right) and its co-crystallized Na_3 calix[4]tube (left). CH hydrogens were omitted for clarity and OH hydrogens are drawn as arbitrary radius spheres. Cyan dashed lines draw hydrogen bonds. Here, Na_3 calix[4]tube was present with three carboxylate groups, which form sealing hydrogen bonds with carboxylic ones. Two other carboxylic groups are inclined outwards the aligned nanotube backbone, which is present with an angle of 4.87(8)° between the average calixarene basal planes, being each one defined as the four crown methylene carbons.

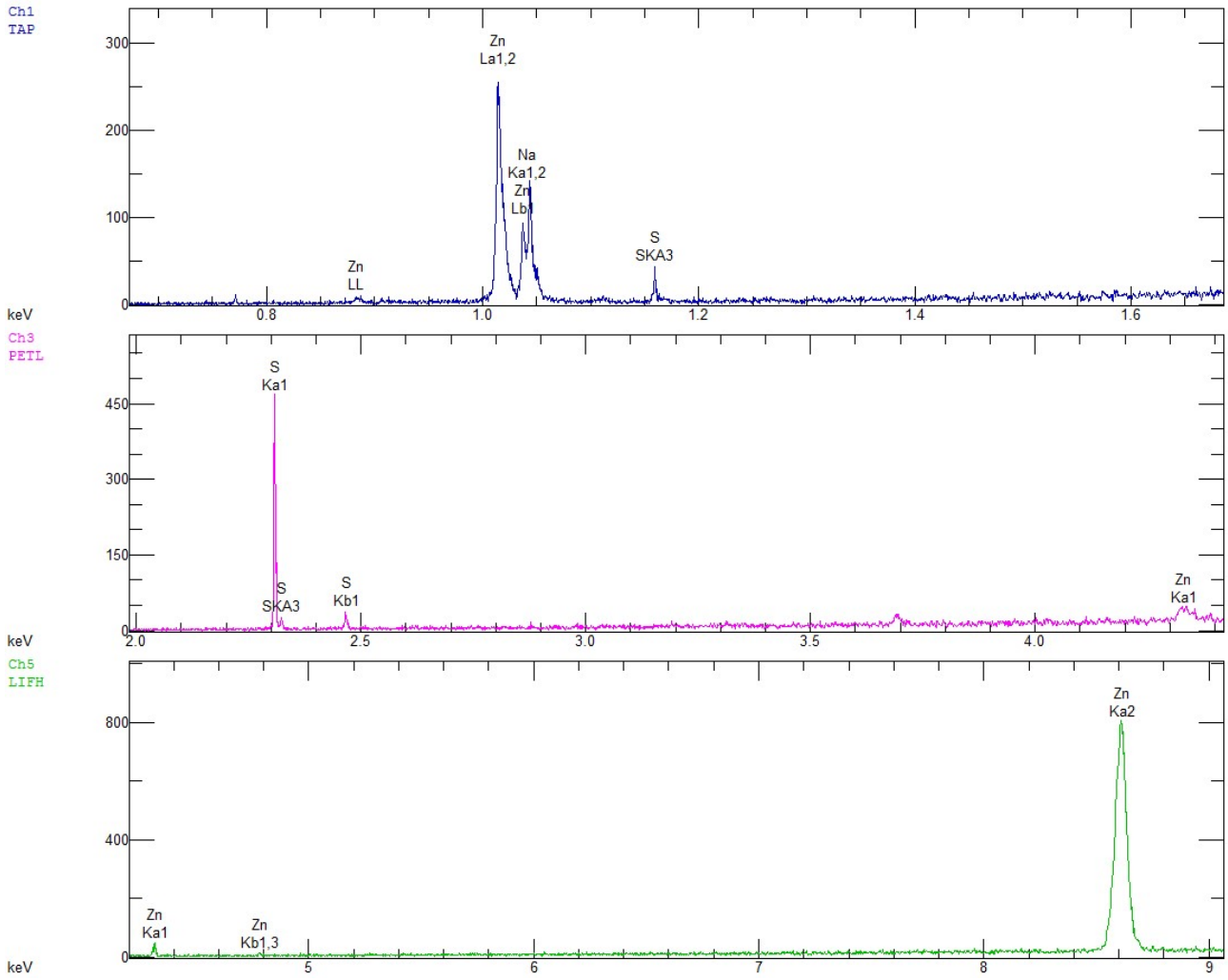

Figure S2. WDS spectrum of a crystal of **2.**

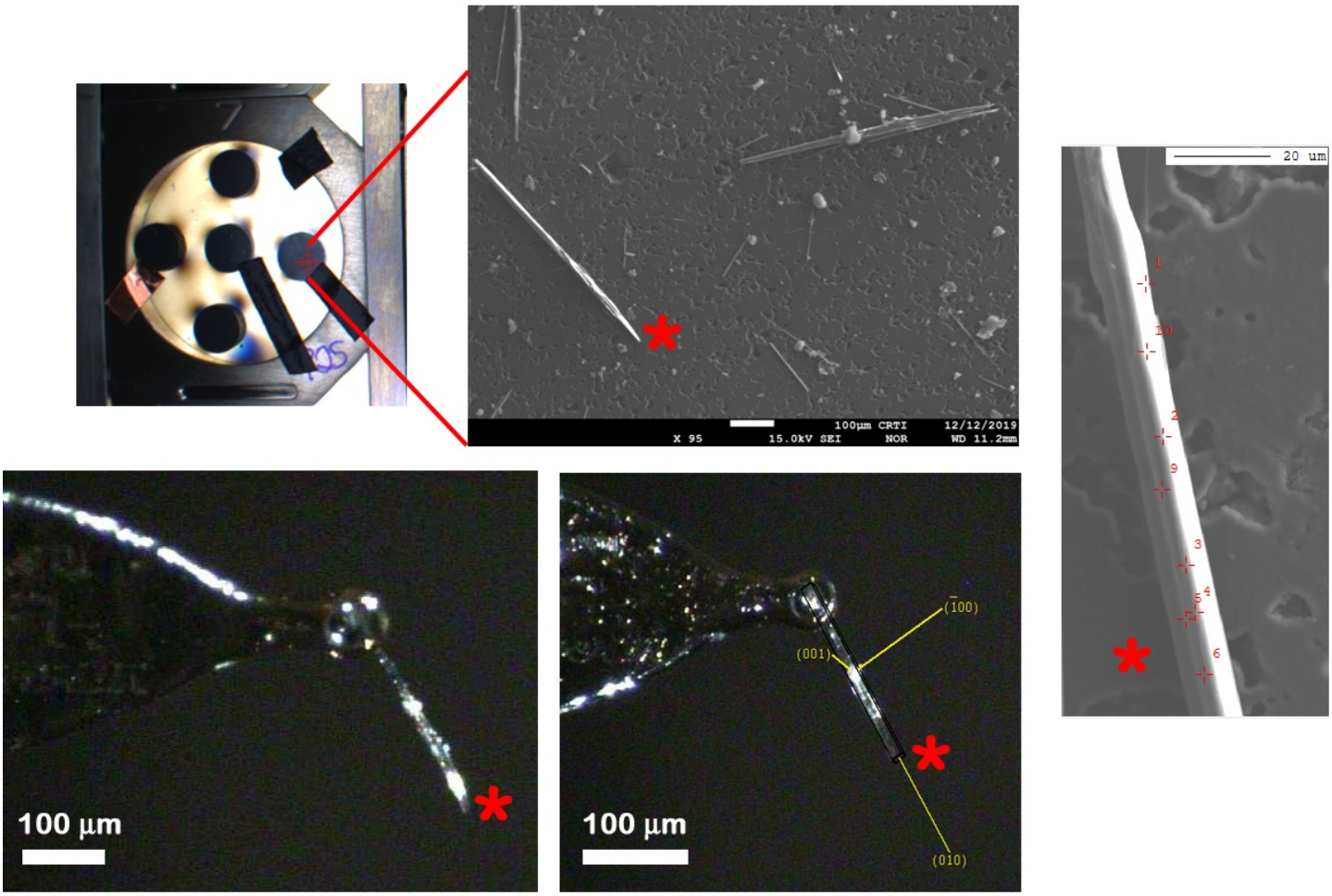

Figure S3. Scanning electron microscopy direct image (top, at centre, and right) of the WDS sample holder with crystals of **2** (top, at left). The asterisk labeled crystal first had its unit cell determined on single-crystal X-ray diffractometer (bottom) and then was carefully placed on the WDS sample holder for image acquisition and spectra measurement. At right, red crosses indicate WDS electron beam 2 µm-sized spots (found Zn/Na molar ratio in the spot number: 1 = 1.49; 2 = 1.32; 3 = 1.31; 4 =1.11; 5 = 1.38; 6 = 1.59; 9 = 1.26; 10 = 1.05; average = 1.32).

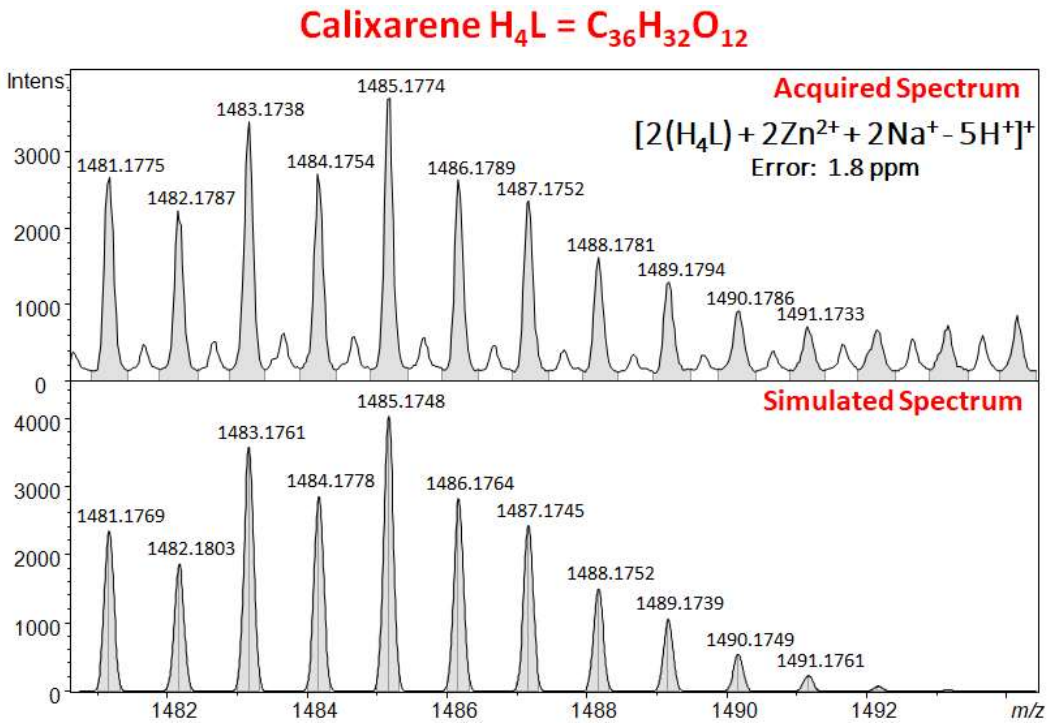

Figure S4. ESI(+) mass spectrum of **1.** Tetramer is disrupted upon ionization, being now each one of the two zinc ions coordinated to only two calixarene units rather than three ones in the crystal structure. For this, the two water molecules are eliminated from both zinc coordination spheres.

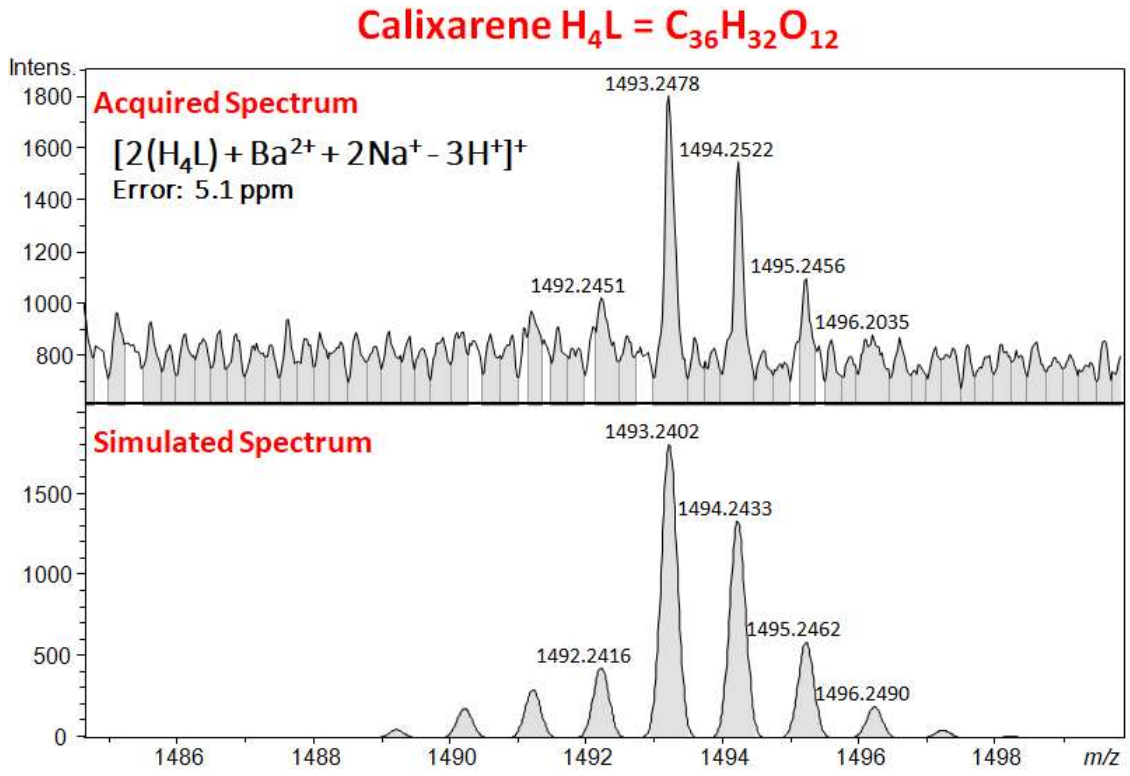

Figure S5. ESI(+) mass spectrum of **3** (molecule B).

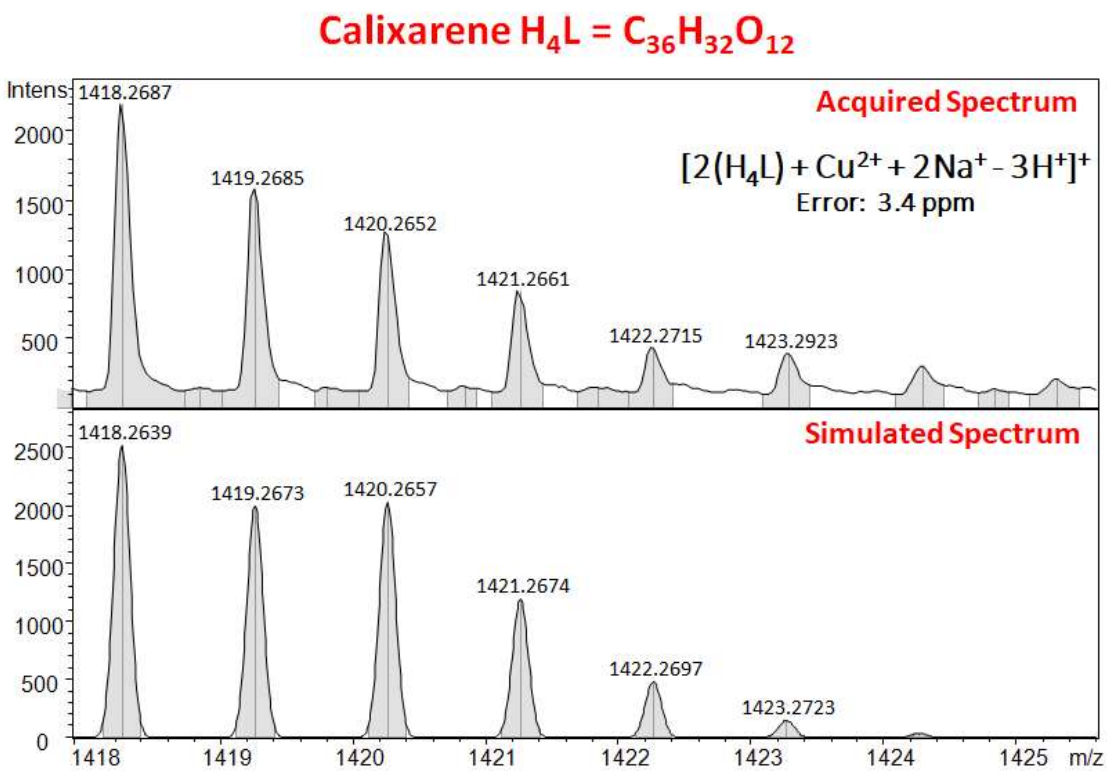

Figure S6. ESI(+) mass spectrum of **4.** Chloride anions were eliminated upon ionization.

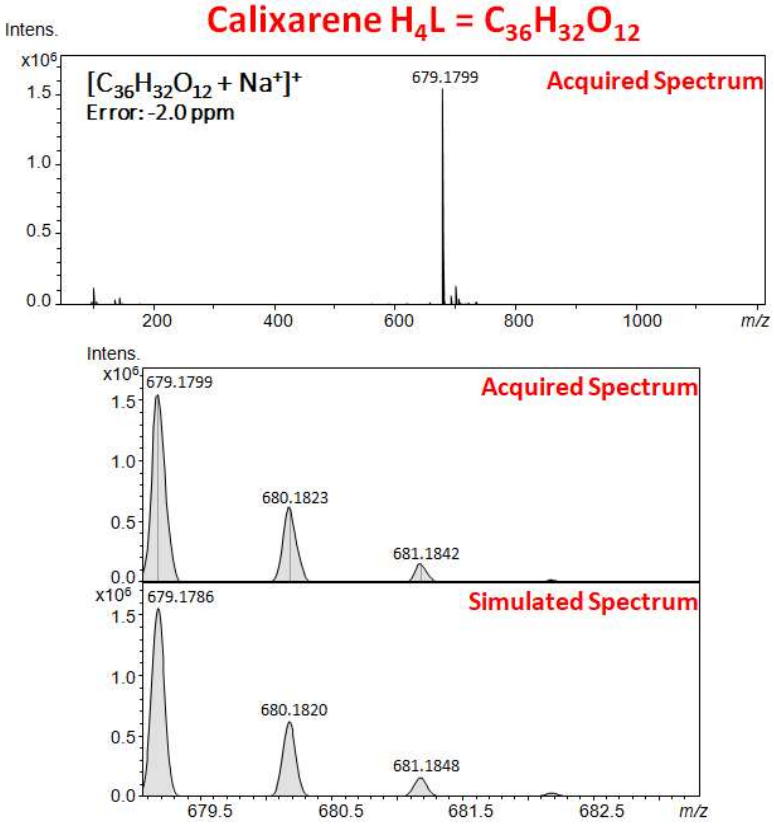

Figure S7. ESI(+) mass spectrum of NaH_3**L**.

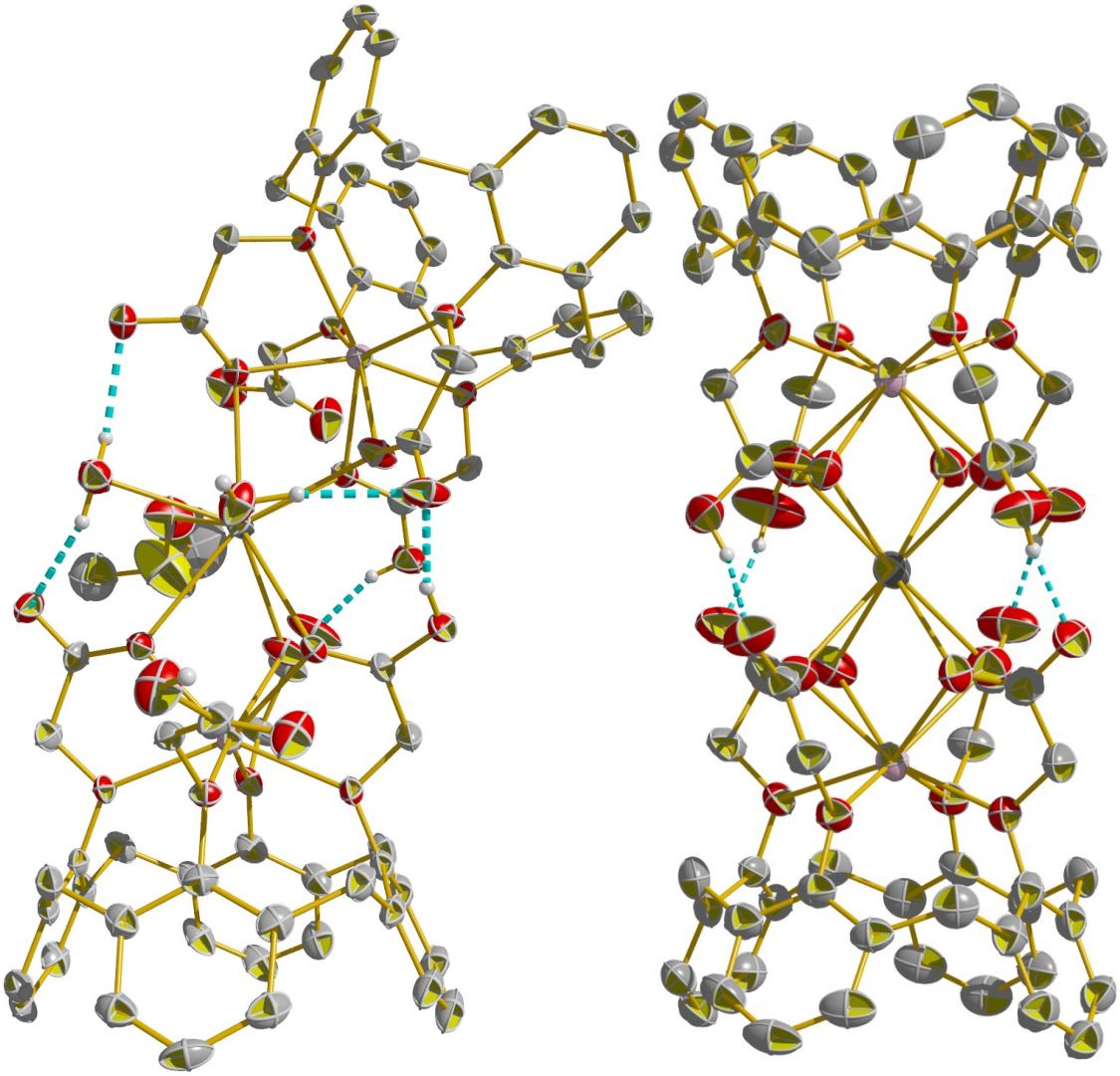

Figure S8. 50% Probability ellipsoids for non-hydrogen atoms of **3** (left, molecule A; right, molecule B). CH hydrogens were omitted for clarity and OH hydrogens are drawn as arbitrary radius spheres. Cyan dashed lines mean hydrogen bonds. There is an angle of 36.93(15)° and 2.17(15)° between the average basal planes of the calixarene units assembling the tubes A and B, respectively (the basal mean plane defined as that crossing through the four methylene carbons bridging phenyl rings). Such a bent-shaping of tube A is due to Ba^{2+} binding pattern differing from that of tube B.

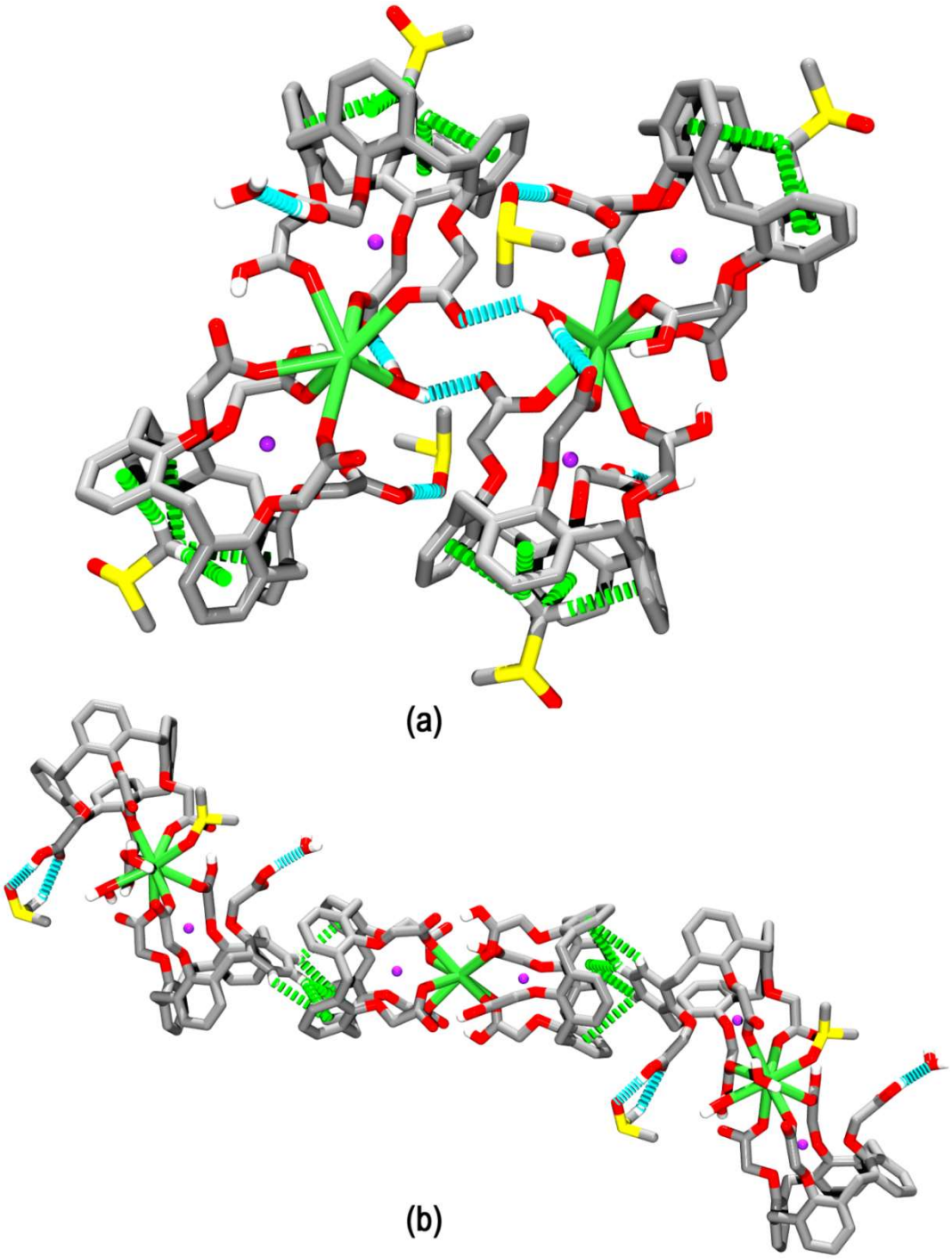

Figure S9. Crystal packing features of **3**. (a) The packing of two calix[4]tubes A in **3** is mediated by intermolecular hydrogen bonding (cyan dashed lines) having coordinated water as donor to carboxylate. In this picture, DMSO entrapping by CH…π contacts can be also viewed (green dashed lines). (b) Central molecule B of **3** hosting phenyl rings of molecule A into its annulus through π…π contacts (green dashed lines). Hydrogen bonds participating carboxylic groups and solvent molecules are also shown in this panel (cyan dashed lines).

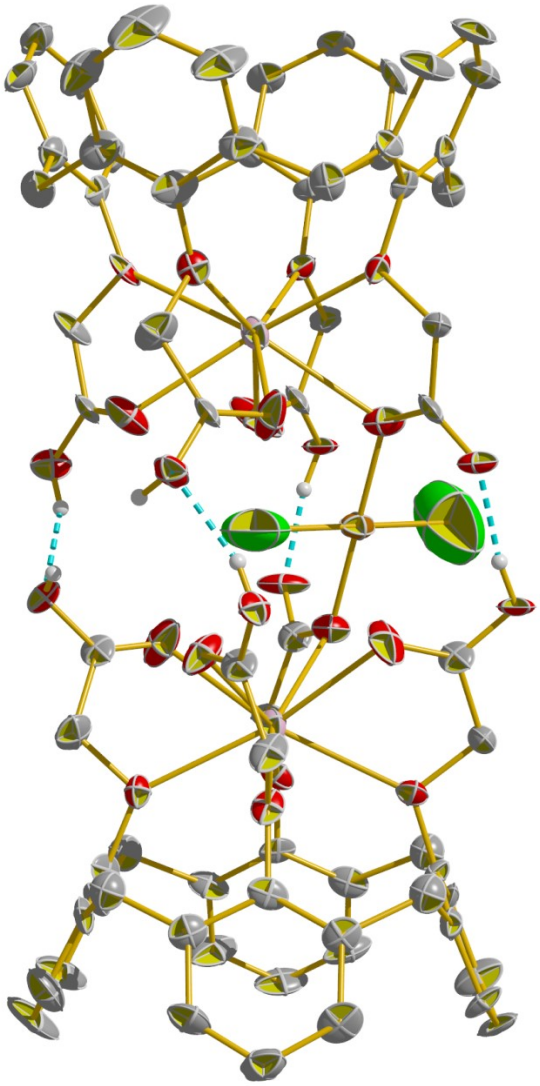

Figure S10. 50% Probability ellipsoids for non-hydrogen atoms of **4.** CH hydrogens were omitted for clarity and OH hydrogens are drawn as arbitrary radius spheres. Cyan dashed lines mean hydrogen bonds.

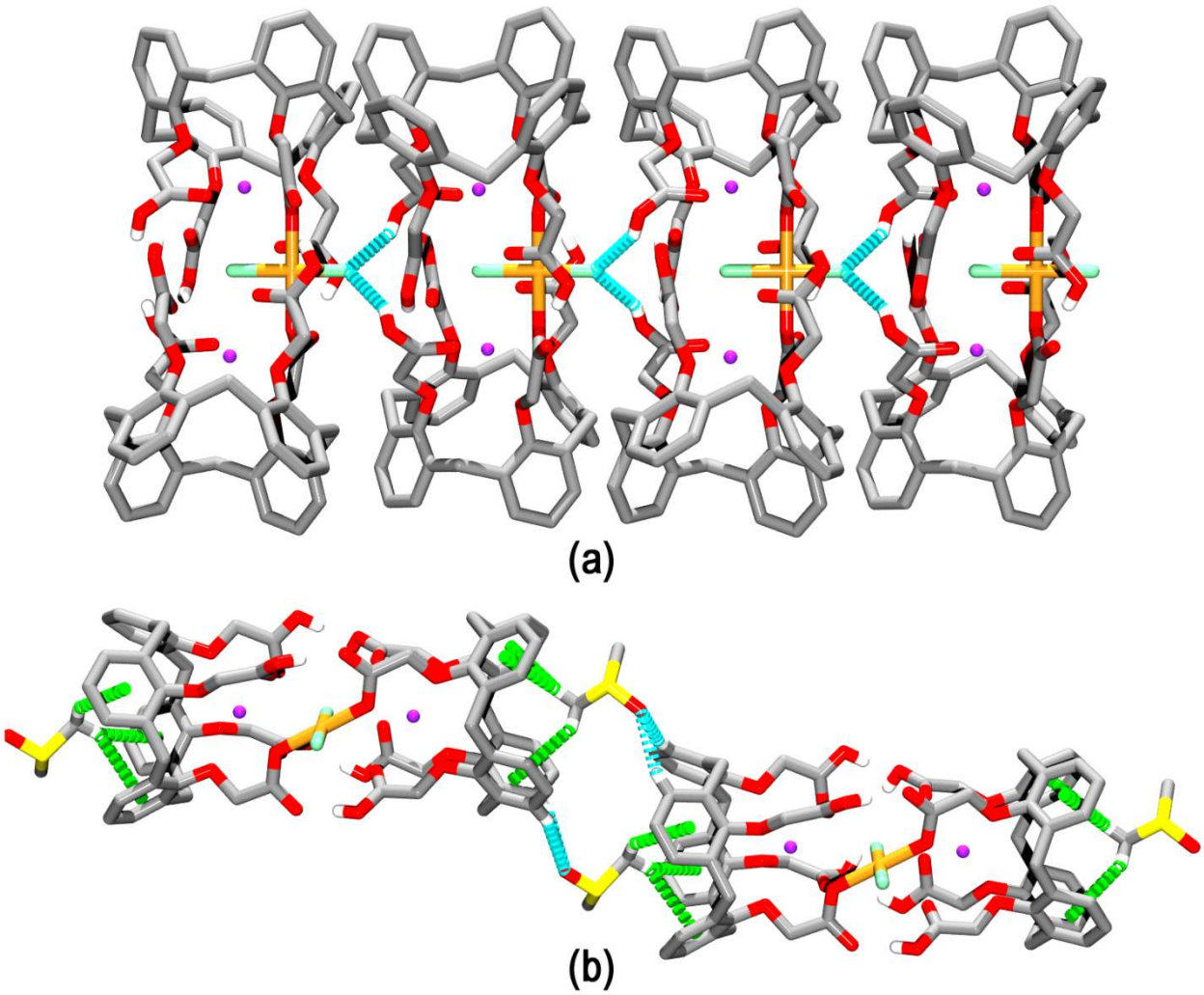

Figure S11. Crystal packing features of **4**. (a) The packing of four calix[4]tubes in **4** is achieved by intermolecular hydrogen bonding (cyan dashed lines) involving carboxylic groups and chloride anions. (b) The entrapping of DMSO into the annulus by CH…π contacts (green dashed lines) and non-classical hydrogen bonds (cyan dashed lines) helping the structure stabilization in **4.**

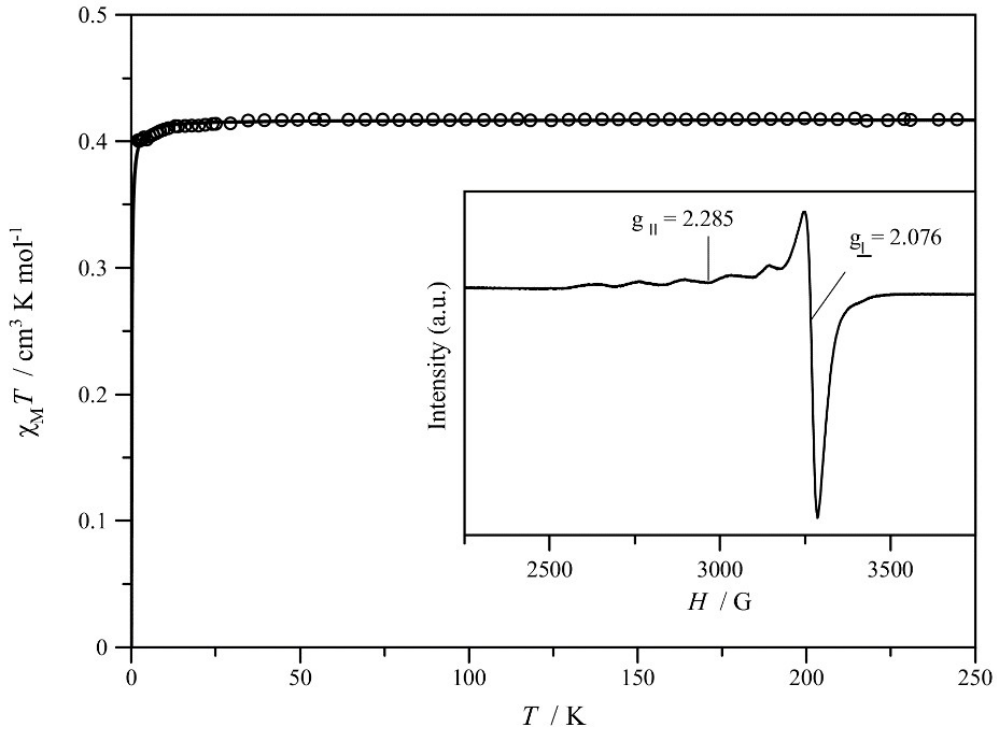

Figure S12. Thermal dependence of $\chi_M T$ for **4**. (○) experimental; (—) best-fit curve through a Curie-Weiss law. The inset shows the X-band EPR spectrum of a polycrystalline sample of **4** recorded at 4.0 K.

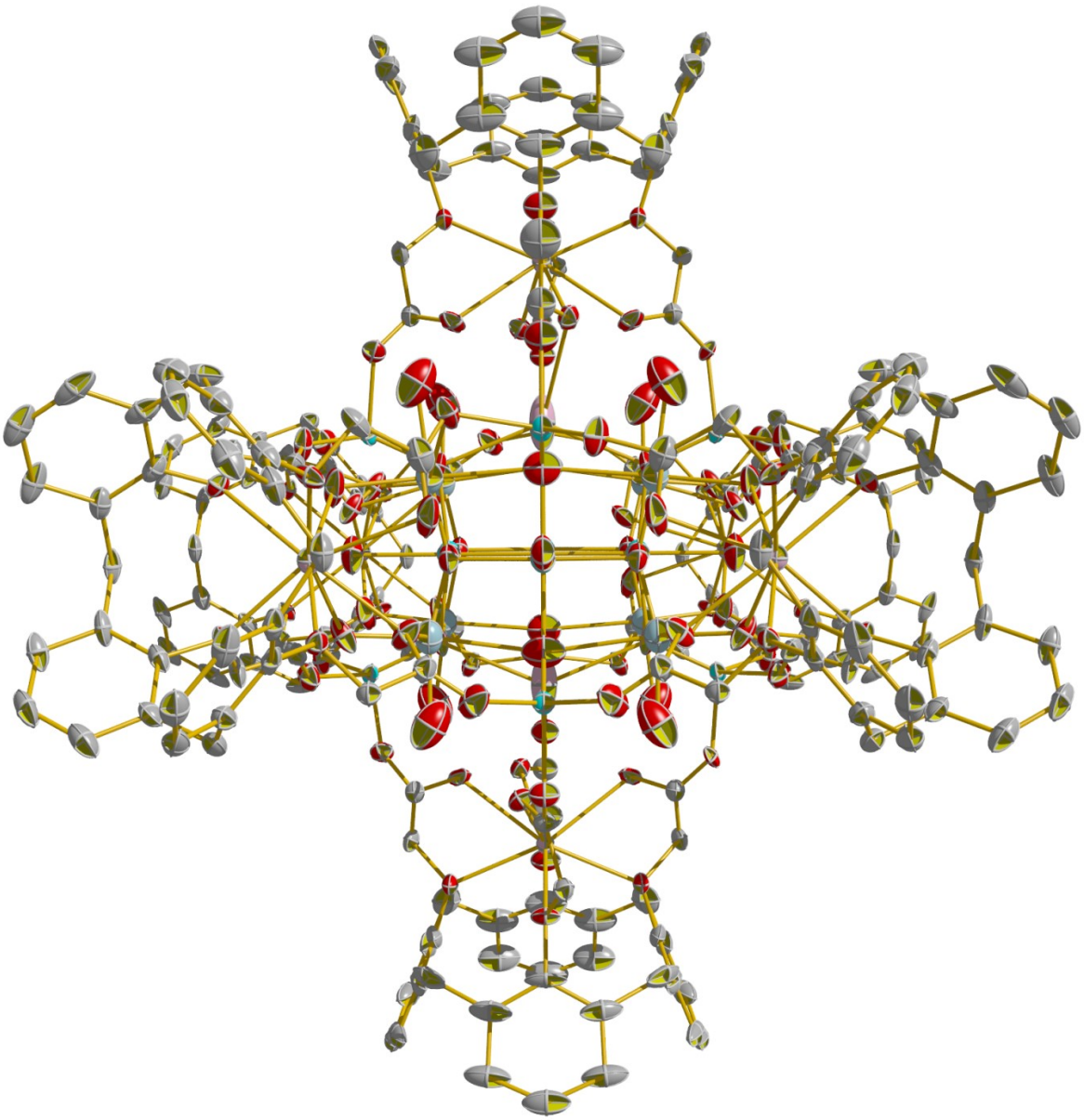

Figure S13. 50% Probability ellipsoids for non-hydrogen atoms of **2.** All hydrogens and disordered non-hydrogen sites with minor or same occupancy were omitted for clarity.

9. References

1 F. T. Martins, C. M. Da Silva, G. A. Vasconcelos, B. Gontijo Vaz, T. D. S. Vieira, L. H. K. Queiroz Júnior and Â. De Fátima, *CrystEngComm,* 2016, **18**, 6987–6991.

2 APEX3, SAINT and SADABS. Bruker AXS Inc., Madison, Wisconsin, USA, 2015.

3 L. Krause, R. Herbst-Irmer, G. M. Sheldrick and D. Stalke, *J. Appl. Crystallogr.,* 2015, **48**, 3–10.

4 G. M. Sheldrick, *Acta Crystallogr. Sect. C,* 2015, **71**, 3–8.

5 L. J. Farrugia, *J. Appl. Crystallogr.,* 2012, **45**, 849–854.

6. O. V. Dolomanov, L. J. Bourhis, R. J. Gildea, J. A. K. Howard and H. Puschmann, J. Appl. Cryst*.,* 2009, 42, 339–341.

7 W. T. Pennington, *J. Appl. Crystallogr.,* 1999, **32**, 1028–1029.

8 J. L. Atwood, L. J. Barbour and A. Jerga, *Science,* 2002, **296**, 2367–2369.

9 R. I. Cooper, R. O. Gould, S. Parsons and D. J. Watkin, *J. Appl. Crystallogr*., 2002, **35**, 168–174.

10 M. E. Alvarenga, A. K. S. M. Valdo, L. Ribeiro, J. A. do Nascimento Neto, D. P. de Araujo, C. M. da Silva, Â. de Fátima and F. T. Martins, *Acta Crystallogr. Sect. C,* 2019, **75**, 667–677.

11 G. Guillemot, E. Solari, C. Rizzoli and C. Floriani, *Chem. Eur. J*., 2002, **8**, 2072–2080.

12 S. G. Wilkinson, R. D. Gillard and J. A. McCleverty, *Pergamon Press,* 1987, pp. 899.

10. Author Contributions

All authors contributed equally to this publication. F.M.S. synthesized and crystallized compounds **1**-**4**. M.E.A., A.K.S.M.V., J.H.A.N., A.A.B., A.P.A. and J.A.E. collected and treated single-crystal X-ray diffraction data. R.R. and D.C.C.G. performed the magnetic analyses and processing for compound **4**. Â.F., T.V.C.L. and C.M.S. performed the synthesis and purification of the ligand calixarene. T.T.T. carried out the MALDI-TOF MS analyses of **2**. V.F.G. and C.M.A.O. analyzed compound **2** by WDS. L.C.S. and B.G.V. analyzed compounds **1**, **3** and **4** by ESI-HRMS. F.T.M. participated supervising all analyses and interpretation besides writing the paper. All authors also contributed in the paper preparation.

11. Acknowledgments

We thank the Brazilian Research Council CNPq (Conselho Nacional de Desenvolvimento Científico e Tecnológico) for the financial support. We are also grateful to Centro Regional para o Desenvolvimento Tecnológico e Inovação (CRTI) for support in WDS analyses. F.T.M., A.F., D.C.C.G., C.M.A.O., B.G.V., A.A.B., A.P.A. and J.A.E. also thank the CNPq for research fellowship. The authors wish to thank Prof. Miguel Julve for very useful remarks and discussions on the reported results. We also thank the Proteomics Core Facility (LMProt) of the Federal University of Minas Gerais (UFMG) and Adriana C. R. Magalhães for the infrastructure and support with the MALDI-TOF MS measurements.